Inorganic Chemistry

Article

pubs.acs.org/IC

Spectroscopic Description of the E₁ State of Mo Nitrogenase Based on Mo and Fe X-ray Absorption and Mössbauer Studies

Casey Van Stappen,[†] Roman Davydov,[‡] Zhi-Yong Yang,[§] Ruixi Fan,[⊥] Yisong Guo,[⊥] Eckhard Bill,[†] Lance C. Seefeldt,[§] Brian M. Hoffman,[‡] and Serena DeBeer*,[†]

[†]Max Planck Institute for Chemical Energy Conversion, Stiftstrasse 34−36, 45470 Mülheim an der Ruhr, Germany
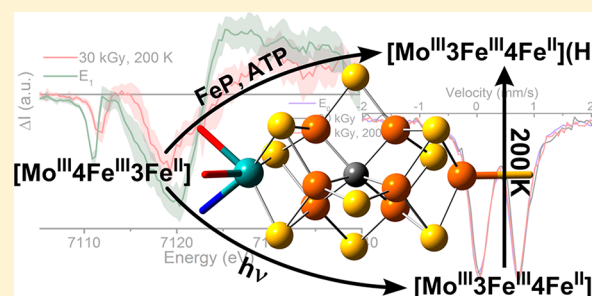[§]Department of Chemistry and Biochemistry, Utah State University, Logan, Utah 84322, United States
[‡]Department of Chemistry, Northwestern University, Evanston, Illinois 60208, United States
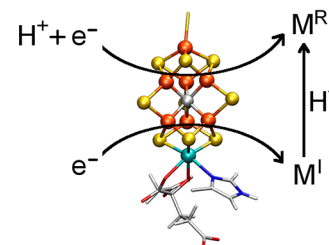[⊥]Department of Chemistry, Carnegie Mellon University, Pittsburgh, Pennsylvania 15213, United States

Ⓢ *Supporting Information*

ABSTRACT: Mo nitrogenase (N2ase) utilizes a two-component protein system, the catalytic MoFe and its electron-transfer partner FeP, to reduce atmospheric dinitrogen (N_2) to ammonia (NH_3). The FeMo cofactor contained in the MoFe protein serves as the catalytic center for this reaction and has long inspired model chemistry oriented toward activating N_2. This field of chemistry has relied heavily on the detailed characterization of how Mo N2ase accomplishes this feat. Understanding the reaction mechanism of Mo N2ase itself has presented one of the most challenging problems in bioinorganic chemistry because of the ephemeral nature of its catalytic intermediates, which are difficult, if not impossible, to singly isolate. This is further exacerbated by the near necessity of FeP to reduce native MoFe, rendering most traditional means of selective reduction inept. We have now investigated the first fundamental intermediate of the MoFe catalytic cycle, E₁, as prepared both by low-flux turnover and radiolytic cryoreduction, using a combination of Mo Kα high-energy-resolution fluorescence detection and Fe K-edge partial-fluorescence-yield X-ray absorption spectroscopy techniques. The results demonstrate that the formation of this state is the result of an Fe-centered reduction and that Mo remains redox-innocent. Furthermore, using Fe X-ray absorption and ^{57}Fe Mössbauer spectroscopies, we correlate a previously reported unique species formed under cryoreducing conditions to the natively formed E₁ state through annealing, demonstrating the viability of cryoreduction in studying the catalytic intermediates of MoFe.

1. INTRODUCTION

The conversion of dinitrogen (N_2) to bioavailable ammonia (NH_3) is a fundamental step in the biogeochemical nitrogen cycle.[1] In nature this process is predominately carried out by nitrogenase (N2ase) enzymes, which have provided the majority of fixed nitrogen for living organisms over the past 2 billion years.[2−4] Perhaps the most efficient and well-studied of these systems is the Mo-dependent enzyme "MoFe", which contains the FeMo cofactor (7Fe-9S-1Mo-1C, commonly referred to as FeMoco; Scheme 1) and the eight Fe containing P-cluster. MoFe functions along with a [4Fe-4S] cluster-containing iron protein (FeP), which serves as the native reductant of MoFe.

Mo N2ase and the FeMoco cluster have long inspired model chemistry for the activation of N_2 and other small molecules. Shortly following the discovery of Mo as an essential component of Mo N2ase,[5] a field of chemistry focused around the tuning of single and polynuclear Mo complexes to bind and reduce N_2 ensued.[6−14] This route has been somewhat successful and has provided some of the first catalytic N_2-activating model complexes.[6,9,11,12,15−22] However, in recent

Scheme 1. Current Proposed Relationship between the Previously Observed Natively Reduced (M^R) and Cryoreduced (M^I) Species Formed at the FeMoco Cluster[a]

[a]Elements are colored as follows: Mo, cyan; Fe, orange; S, yellow; N, blue; O, red; C, gray.

years, the focus has turned to Fe because numerous spectroscopic (as well as crystallographic) studies show that substrate binding occurs at a four-Fe face (Fe2,3,6,7) of

FeMoco and not at Mo.[23−28] Nevertheless, whether or not Mo plays any role in redox chemistry under native reducing conditions has yet to be established, as does the potential role of Mo during the N_2 reduction stages.

During the catalytic cycle, stepwise electron transfer is coupled to the transfer of a proton to create intermediates denoted as $E_n(nH)$, where n is the number of electron-transfer steps (Scheme 2). The ratios of these intermediates to one

Scheme 2. Simplified Depiction of the Kinetic Mechanism of Mo-Dependent N2ase Describing the Relationships between the Catalytic Intermediates E_n, in Which n Represents the Number of Electrons/Protons Delivered to FeMoco from FeP^a,[29−32]
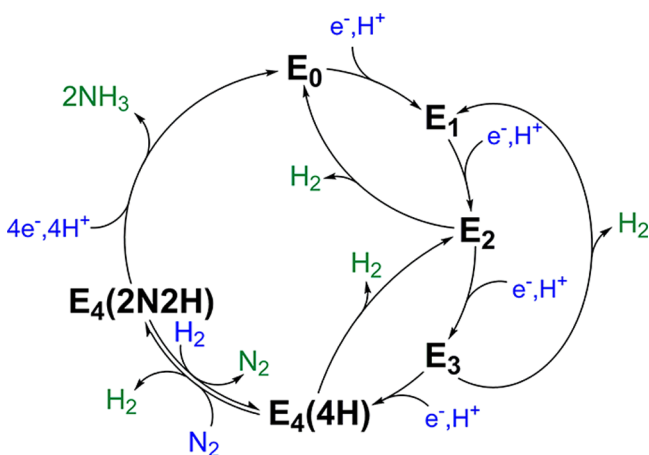
^{a}The number of added protons and N atoms is indicated for $n = 4$.

another are dependent on the rate of electron transfer versus dihydrogen (H_2) production from the states $E_2–E_4$ and can be influenced by adjusting the ratio of MoFe/FeP during turnover. H_2 can be produced at any point in which at least two electrons and protons have accumulated.[29−32] In the absence of N_2, the cycle is limited to the population of intermediates $E_0–E_4$.

The presence of this distribution of intermediate states during catalytic turnover has made the trapping of individual intermediate species particularly difficult. This problem has been partly overcome by the use of electron paramagnetic resonance (EPR) and electron nuclear double resonance/electron spin-echo envelope modulation (ENDOR/ESEEM) methods to study these intermediates, which have established that N_2 reduction to $2NH_3$ requires 8 equiv of H^+ and $e^−$, along with 16 ATP, as proposed earlier,[3,33−36] to bind N_2 and cleave the triple bond of nitrogen at FeMoco to produce two molecules of NH_3 (eq 1).[4,37,38]

$$N_2 + 8e^- + 16ATP + 8H^+$$

$$\rightarrow 2NH_3 + H_2 + 16ADP + 16P_i \qquad (1)$$
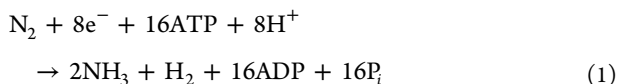
As indicated in Scheme 2, during its catalytic cycle, N2ase is activated to reduce the N≡N triple bond by the accumulation of $n = 4$ $e^−/H^+$, followed by the reductive elimination of H_2 coupled to N_2 binding/reduction.

The EPR and ENDOR/ESEEM methods used to achieve these results are limited to odd-electron E_n intermediates. The resting state of FeMoco is odd-electron, meaning that these methods were restricted to n-even states, leaving the n-odd

states unexamined. Beyond the need for ways to address these states, methods that are capable of selective reduction of the FeMoco cluster would be highly valuable for studying all intermediates. This has been no easy task, and while progress has been made in reducing MoFe in the absence of FeP,[39−43] there is still no precedence for chemical or electrochemical means of single-electron reduction. To this end, cryoreduction has already offered a promising route to accessing n-even states in the accumulation phase of Mo N2ase ($E_0–E_4$).[44,45] Cryoreduction involves the direct injection of a radiolytically produced mobile electron into a metal center or cluster at 77 K. Previously, this technique was successfully used to decouple electron- and proton-transfer steps when moving between the E_0 and E_2 states of FeMoco.[45] This technique has also been previously applied in the ^{57}Fe Mössbauer spectroscopy investigation of several oxidation states of Mo N2ase, where it was proposed that native turnover resulted in a Mo-centered reduction, while cryoreduction produced an alternative Fe-reduced state.[46]

It is well-known from the pioneering work of Lowe and Thorneley that both electron and proton transfer to the FeMoco cluster occur during native turnover.[29−32] This provides the opportunity for protonation of either a sulfur or iron in the FeMoco cluster. While spectroscopic characterization of the E_1 and E_3 states has remained minimal due to their non-Kramers spin states, intensive ENDOR studies support the formation of Fe-hydride species in the E_2 and E_4 states.[38,47,48] From logical deduction, it is also possible that the E_1 state involves the formation of a metal-hydride species, making this an alternative to the protonation of a cluster sulfide (Scheme 3). Metal-hydride species are generally highly

Scheme 3. Proposed States and Relationships between the E_0, E_1, and E_2 States of Mo N2ase^a
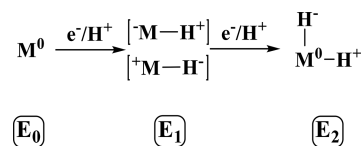
^{a}"M" is used to simply denote the entire FeMoco cluster rather than a particular binding site.

covalent, making it possible for the average electron density at iron in a metal-hydride containing E_1 state to appear very similar or even more oxidized than that of E_0. Similarly, protonation of an inorganic sulfide in the cluster may also skew the electron density at Fe despite being formally reduced. In this sense, protonation of either Fe or S may serve to maintain a similar reduction potential for each E_n state, allowing the catalytic cycle to advance.[4] Given these considerations, it may be that the discrepancies between the originally reported[46] native turnover and cryoreduced species arise not from a change in the locale of reduction but because the cryoreduced state has not acquired a proton, and that follow-up protonation of FeMoco generates the E_1 state (as illustrated in Scheme 1).

Herein, we employ a series of spectroscopic methods to elucidate the nature of the E_1 and cryoreduced states of MoFe. We have employed low-flux turnover conditions ([MoFe]: [FeP] = 50:1) to generate favorable quantities of the E_1 state, using X-band EPR to monitor the decrease of E_0 and ensure that further reduced species are not formed. High-energy-resolution-fluorescence-detected (HERFD) and partial-fluo-

rescence-detected (PFY) X-ray absorption spectroscopy (XAS) techniques are employed as element-selective and oxidation-state sensitive probes of Mo and Fe to elucidate the redox-active centers of the FeMoco cluster and provide insight into the relationship between the cryoreduced and native turnover states. Finally, ^{57}Fe Mössbauer spectroscopy is used to reconcile the past and present observations of reduced FeMoco.

2. MATERIALS AND METHODS

Materials and Protein Purifications. All reagents were obtained from Sigma-Aldrich (St. Louis, MO) or Fisher Scientific (Fair Lawn, NJ) and used without further purification. Ar and N_2 gases were purchased from Air Liquide America Specialty Gases LLC (Plumsteadville, PA) and passed through an activated Cu catalyst to remove any traces of dioxygen before use. *Azotobacter vinelandii* strains DJ995 (wild-type MoFe protein with a His tag) and DJ 884 (wild-type FeP protein) were grown, and the corresponding His-tagged MoFe and FeP proteins were expressed and purified as described previously.[49] The protein concentrations were determined by Biuret assay. The purities of these proteins were >95% based on sodium dodecyl sulfate polyacrylamide gel electrophoresis analysis with Coomassie staining. The MoFe and Fe proteins were fully active with specific activities. All manipulations of the proteins and buffers were performed in septum-sealed serum vials under an Ar atmosphere or on a Schlenk vacuum line. All liquids were transferred using gastight syringes.

Preparation of Cryoreduced Samples. Samples prepared for irradiation consisted of 520 μM MoFe in 100 mM 3-(*N*-morpholino)propanesulfonic acid (MOPS), 200 mM NaCl, and 20 mM sodium dithionite at pH 7.3 with 5% glycerol by volume. All samples in XAS sample holders were frozen and stored in liquid nitrogen before cryoreduction and further measurements. γ irradiation of the N2ase samples at 77 K was performed for approximately 6 h at a time (5 kGy h^{-1} for a 30 kGy total dose) using a Gammacell 220 ^{60}Co source. Annealing at 200 K was performed by placing samples in a liquid N_2/pentane bath (cooled to 200 K) for 2 min, followed by refreezing in liquid N_2. Reduction of E_0 was monitored via EPR by reduction in the amplitude of the E_0 $S = {}^3/_2$ signal at $g_{max} = 4.34$. Cryoreduced samples are denoted in the following text by their dose and annealing temperature (if annealed). For example, "30 kGy" refers to an unannealed sample of MoFe, which has been exposed to 30 kGy of radiation, while "30 kGy, 200 K" refers to a sample that has been irradiated with 30 kGy of radiation, followed by annealing at 200 K for 2 min.

Preparation of Native Turnover Samples. All native turnover XAS samples were prepared in a 200 mM MOPS buffer at pH 7.3 with an MgATP regeneration system (12 mM $MgCl_2$, 20 mM phosphocreatine, 10 mM ATP, 1 mg mL^{-1} bovine serum albumin, and 0.4 mg mL^{-1} creatine phosphokinase), 50 mM NaCl, 50 mM sodium dithionite, and 5% (v/v) glycerol under Ar. The MoFe protein was added to a final concentration of 400 μM, and the reaction was initiated by the addition of FeP protein to a final concentration of 8 μM. After incubation at room temperature for about 10 min, the reaction mixture was transferred into the XAS sample holder and freeze-quenched in liquid N_2. Samples were stored and shipped in liquid N_2.

EPR Measurements. EPR spectra were recorded using a Bruker X-band ESP 300 spectrometer with an Oxford Instruments ESR 900 continuous-flow cryostat at 10 K. Quantitation of E_0 reduction was performed by measuring the decrease in the intensity of the g_1 feature at 4.34 of reduced samples relative to that of the resting state (see section S2 of the Supporting Information for measurements performed on the samples used for XAS measurements). This is possible because the intrinsic line width of the E_0 $S = {}^3/_2$ signal and measurement conditions for each of these samples are identical. These results are corroborated by spin-integration (Table S1).

HERFD XAS Measurements. HERFD XAS data of all N2ase samples were obtained at the ID26 beamline at the European Synchrotron Radiation Facility (ESRF). The storage ring operated at 6 GeV in 16-bunch top-up mode and ~90 mA ring current. A double-crystal monochromator using Si(311) crystals was used to select the incoming X-ray energy with an intrinsic resolution ($\Delta E/E$) of 0.3 × 10^{-4}. A liquid-He-flow cryostat was maintained at approximately 20 K in order to minimize radiation damage and to maintain an inert sample environment. A 1-m-radius multicrystal Johann-type X-ray spectrometer was used to select the energy of the emitted X-rays and record HERFD XAS data using a dead-time-corrected Ketek Si drift diode detector in a Rowland geometry. Standard XAS was also collected by total fluorescence yield simultaneously with HERFD measurements.

In the Mo XAS measurements, the energy of the incoming X-rays was calibrated by recording the transmission K-edge XAS spectrum of a Mo foil and assigning the energy of the maximum of the white line to 20016.4 eV. For Mo Kα HERFD measurements, the spectrometer was equipped with five curved Ge(111) crystals positioned at a Bragg angle of 77.74°, utilizing the [999] reflection to focus the Mo Kα_1 emission (~17480 eV) on the detector. Short XAS scans were collected by scanning the incident energy from 19990 to 20090 eV, while long XAS scans obtained for normalization were collected from 19910 to 20910 eV. Prior to measurements, each sample was checked for signs of radiation damage by performing subsequent short XAS scans from 19990 to 20090 eV on the same sample spot, using a rate of 5 s per scan. These tests showed that MoFe was stable under X-ray irradiation at the Mo K-edge for >300 s.

All Fe XAS measurements were calibrated by aligning the first inflection point of the HERFD XAS spectrum of a 10-μm-thick α-Fe foil layered in Kapton tape to 7111.2 eV. The spectrometer was equipped with five curved Ge(110) crystals positioned in a Roland geometry at a Bragg angle of ~68°, using the [440] reflection to focus the Fe Kα_1 emission (7467 eV) on the detector. Short XAS scans were collected by scanning the incident energy from 7100 to 7200 eV, while long XAS scans obtained for normalization were collected from 6930 to 7920 eV. Prior to measurements, each sample was checked for signs of radiation damage by performing subsequent short XAS scans from 7100 to 7200 eV on the same sample spot, using a rate of 5 s per scan. These tests showed that MoFe was stable under X-ray irradiation at the Fe K-edge for up to 120 s.

PFY XAS Measurements. XAS measurements of intact N2ase MoFe and Fe proteins were obtained at the 9-3 beamline of the Stanford Synchrotron Radiation Lightsource (SSRL). The SPEAR storage ring operated at 3.0 GeV in a top-off mode with a 500 mA ring current. A liquid-N_2-cooled double-crystal monochromator using Si(220) crystals at $\phi = 0°$ was used to select the incoming X-ray energy with an intrinsic resolution ($\Delta E/E$) of 0.6 × 10^{-4}, and a Rh-coated mirror was used for harmonic rejection. The X-ray beam size was 1×4 mm^2 ($V \times H$) at the sample position. A liquid-He-flow cryostat was used to maintain at approximately 20 K sample environment in order to prevent radiation damage and maintain an inert sample environment. Fluorescence measurements were recorded using a Canberra 100-element Ge monolith solid-state detector. Prior to measurements, each sample was checked for signs of radiation damage by performing subsequent 5 min scans over the same sample spot. These tests showed that MoFe was stable under X-ray irradiation at the Mo K-edge for >90 min and at the Fe K-edge for >70 min.

Energy calibrations for the Mo and Fe K-edge XAS measurements were performed by recording the transmission K-edge XAS spectra of Mo and Fe foils, respectively, and assigning their energies, as detailed above in the HERFD XAS Measurements section. Full XAS scans at the Mo K-edge were collected by scanning the incident energy from 19780 to 21142 eV. All Fe XAS scans were collected by scanning the incident energy from 6882 to 8093 eV. Calibrations for each individual scan at both Mo and Fe K-edges were recorded simultaneously by measurements of the transmission of the respective metal foils.

XAS Data Processing. For all HERFD experiments, individual scans were normalized to the incident photon flux and averaged using PyMCA.[50] Further processing of all spectra, including background subtraction and normalization, was performed using the *Athena* program from the software package *Demeter*,[51] following standard protocols for X-ray spectroscopy.[52,53] Background subtraction and normalization of the averaged Mo XAS spectra was performed using a linear regression for the preedge region of 19910−19947 eV and a quadratic polynomial regression for the postedge region of 20157−20807 eV. The Fe XAS spectra were processed in a fashion similar to that of the Mo XAS spectra. Background subtraction and normalization were performed using a linear regression for the preedge region of 6990−7005 eV and a quadratic polynomial regression for the postedge region of 7160−8200 eV. Statistical analyses of XAS measurements were performed by normalization of individual scans based on the edge area, followed by calculation of the standard deviation based on the deviation of individual scans from the average of all scans (eq 2).

$$\sigma = \sqrt{\frac{\sum_i^j (x_i - x_{av})^2}{j-1}} \tag{2}$$

where σ is the standard deviation, x_i is an individual scan, x_{av} is the average over all scans, and j is the total number of scans.

All spectral subtractions and manipulations were performed using normalized spectra. All XAS spectra in the main text are presented as "pure" spectra, in which contributions from the remaining resting (E_0) state MoFe have been subtracted from the observed spectrum and the resulting spectrum of the "pure" species has been renormalized. The amount of remaining E_0 in a given sample is based on the relative intensity of the E_0 $S = {}^3/_2$ signal (as determined by EPR) relative to that of the resting state. Standard errors resulting from spectral subtractions involving removal of the resting state E_0 contribution were propagated using eq 3:

$$\sigma_{x_a - x_b} = \frac{1}{1 - x_b} \sqrt{x_a^2 \sigma_a^2 + x_b^2 \sigma_b^2} \tag{3}$$

where $\sigma_{x_a - x_b}$ is the standard deviation of the renormalized spectrum generated by the subtraction of fraction x_b of spectrum "b" from spectrum "a". In all cases, $x_a = 1$. Where difference spectra are presented, in which $x_b = 1$, eq 3 simplifies to

$$\sigma_{a-b} = \sqrt{\sigma_a^2 + \sigma_b^2} \tag{4}$$

^{57}Fe Mössbauer Spectroscopy Measurements. ^{57}Fe Mössbauer spectra were recorded with a spectrometer using a Janis Research (Wilmington, MA) SuperVaritemp dewar, which allows studies in applied magnetic fields up to 8.0 T in a temperature range of 1.5−200 K. Isomer shifts are quoted relative to the α-Fe metal at 298 K. Mössbauer spectral simulations were performed using the local program *mf* (available from E.B.) using the minimum number of necessary quadrupole doublets to gauge the average isomer shift of each spectrum. The preparation of the resting state ^{57}Fe Mössbauer sample was previously described.[46]

3. RESULTS

EPR. During turnover in the absence of N_2, the enzyme only accesses the E_0−E_4 states while generating H_2, as depicted in Scheme 2. The EPR signals from the several E_2 and E_4 states are well characterized.[4,37,38] Therefore, any intensity that is unaccounted for in the continuous-wave (CW) EPR when comparing samples of the resting E_0 state and a turnover state can be associated with population of the E_1 and E_3 states. In the present study, low-electron flux conditions (enabled by a high [MoFe]:[FeP] ratio) have slowed reduction of the cluster to the point that the rate of H_2 production from E_2 is greater than the rate of E_2 formation. This results in the population of only the E_0 and E_1 states, as confirmed by the absence of

signals associated with the E_2 state in any of the samples used in the present study (Figure S1).[45,54]

Cryoradiolysis at 77 K has previously been found to not only reduce the FeMoco cluster but also partially oxidize the P cluster despite the presence of glycerol, which favors the former.[45] Figure 1 shows the persistence of the $S = {}^1/_2$ signal (g
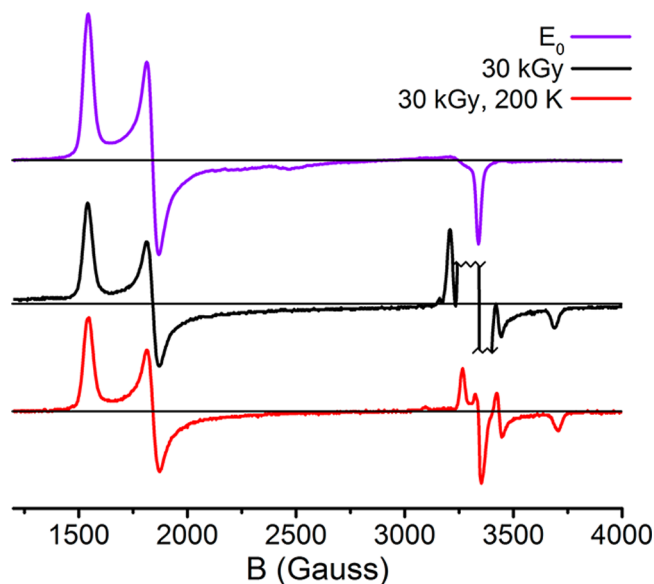

Figure 1. X-band CW EPR spectra of resting MoFe (E_0), 30 kGy cryoreduced, and 30 kGy, 200 K annealed samples. The $g \sim 2$ region of the 30 kGy spectrum is abbreviated because of the presence of large radical signals; these arise from free radicals generated by the irradiation procedure. Measurements were performed at 10 K, 9.371 GHz using a power of 2 mW and a 13 G modulation amplitude.

= 2.05, 1.95, and 1.81)[55] corresponding to P^+ in the cryoreduced samples, even after annealing at 200 K. The contribution of P^+ can be roughly quantified based on the intensity of this feature relative to the $S = {}^3/_2$ E_0 signal (see section S2 of the Supporting Information for details). In doing so, we find that approximately 7% of the P cluster is oxidized in the irradiated samples.

On the basis of such intensity measurements, samples trapped during turnover under Ar contain ∼55% E_0, and the remaining ∼45% is assigned to E_1, while resting-state samples cryoreduced with 30 kGy contain ∼60% E_0 (and, therefore, ∼40% E_1) and ∼7% P^+ (Table S1).

Mo Kα HERFD XAS. A discussion of the changes that occur at the Mo K-edge upon reduction is provided in section S3 of the Supporting Information and demonstrated with a series of model complexes. Briefly, a one-electron reduction of Mo^{III} is expected to result in a ∼ 1 eV decrease in energy of the edge, while the some variation in the preedge region is expected to occur depending on competing factors of centrosymmetry versus a reduced number of available holes in the valence shell.[56] Upon inspection of Figure 2, we find that no significant changes occur in the Mo spectrum of MoFe during either native turnover (E_1), following cryoreduction (30 and 60 kGy), or annealing of the cryoreduced sample (30 kGy, 200 K). While some slight variation occurs in the edge around 20010 eV, these changes are well within the standard error of the experiment (Figure S5) and not of the appropriate magnitude to substantiate an oxidation state change at Mo.
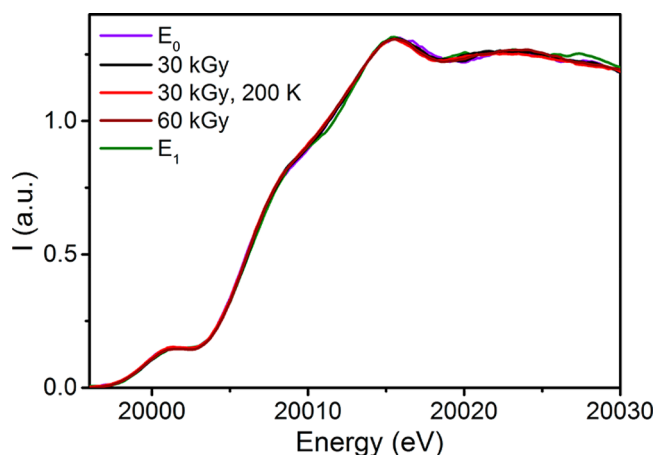
Figure 2. Comparison of the normalized Mo $K\alpha$ HERFD XAS spectra of the MoFe samples under investigation. All XAS spectra (besides E_0) are presented as renormalized "pure" species, in which any remaining E_0 component (as determined by EPR, see section S2 of the Supporting Information) has been subtracted from the experimentally observed spectrum. Prior to any spectral subtractions, an 11-point boxcar average smoothing was applied.

Hence, in E_0, natively reduced, and cryoreduced MoFe samples, Mo remains Mo^{III}.

Fe K-Edge XAS Considerations. Because XAS is a bulk technique and there are up to three unique Fe−S clusters present in these samples, it is naturally necessary to determine whether spectral changes that occur upon reduction are attributable to the FeMoco cluster, P-cluster, FeP, or some combination. During native turnover, single-electron transfer is accomplished in a stepwise fashion that is initiated by the binding of the reduced, ATP-bound form of the Fe N2ase protein (FeP^{red}). This binding event induces a conformationally gated one-electron transfer from the P-cluster to FeMoco, followed by the a one-electron transfer from FeP^{red} to P$^+$ in what is referred to as a "deficit spending" electron-transfer process.[57,58] This is followed by hydrolysis of ATP to ADP, the release of two P_i, and subsequent dissociation of FeP^{ox}.[59] This series can be summarized as follows:

$$FeMoco/P/FeP^{red} \rightarrow FeMoco^-/P^+/FeP^{red}$$

$$\rightarrow FeMoco^-/P/FeP^{ox}$$
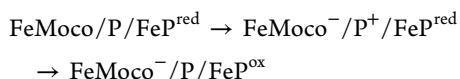
Backfilling electron transfer from FeP^{red} to P$^+$ occurs rapidly relative to the transfer from P to FeMoco.[57] Therefore, under native turnover conditions, the bulk oxidation state of the P cluster remains invariant. In the native turnover samples used here, a 50:1 ratio of [MoFe]/[FeP] is used. Hence, FeP accounts for just 0.27% of the total Fe in these samples, and therefore the contribution of either FeP^{red} or FeP^{ox} to the native turnover spectrum is negligible.

The cryoreduced samples lack FeP but exhibit the presence of a relatively small quantity of a one-electron-oxidized P cluster. Previous XAS studies of P^{ox} have shown this species to have a decreased white-line intensity relative to P^N between 7122 and 7132 eV, as well as small increases in the intensity at both the preedge and edge (Figure S20).[60]

Fe $K\alpha$ HERFD and PFY. The Fe $K\alpha$ HERFD of MoFe under cryoreducing conditions is provided in section S4 of the Supporting Information. Briefly, cryoreduction only results in minor increases in the intensity of the white-line region from 7125 to 7135 eV of approximately 1.2−2% of the total

normalized intensity (Figure S4) when observed with this technique. This small degree of change is not surprising because 15 unique Fe centers contribute to MoFe, and formally we expect a single-oxidation-state change for one of these centers. On the basis of studies of model complexes and comparisons of the VFe and MoFe proteins, a white-line increase between 0.5 and 10% can be anticipated.[61] This is also discussed in greater detail in section S4 of the Supporting Information.

One of the powerful advantages of HERFD XAS lies in its line-sharpening effect, a result of the narrow experimental energy bandwidth approaching that of the intrinsic lifetime broadening of the fluorescent event being observed.[62,63] This is particularly useful for measurements of elements with larger Z (such as Mo), which have shorter 1s core−hole lifetimes and therefore greater lifetime broadening (as demonstrated in Figure S6).[64] While line sharpening also occurs at Fe, it is less pronounced because of its longer core−hole lifetime.

Meanwhile, one of the primary *disadvantages* of HERFD is its utilization of an intrinsically small solid angle; this is necessary to select the very narrow range of fluorescent energies used in detection at the Kα line.[65] This means that the amount of signal observed in HERFD measurements is usually quite low, making an intense, high-flux incoming X-ray beam necessary to produce substantial count rates. In turn, rapid scan times must be used to mitigate the damage that such a high-flux incident beam inflicts on the sample.[52] When this is combined with the low count rates, which result from dilute protein solutions, the level of noise in individual scans becomes considerable. In the present case, despite extensive collection times, the statistical uncertainty in these spectra remains considerably greater than the small differences observed between the resting and cryoreduced/annealed samples. Figure S9 provides the difference spectra of the 30 and 60 kGy samples, where the standard error of these experiments ranges around ±2−3%.

To overcome the challenges presented when observing such a small degree of change (again, 1.2−2%), we elected to employ standard Fe K-edge PFY XAS to provide insight into the relationship between the resting, cryoreduced, and natively reduced systems. PFY XAS measurements utilize a larger solid angle and collect emitted fluorescent photons over a much larger range of energies, providing approximately an order of magnitude higher count rates than those observed by HERFD for similar samples. Additionally, significantly longer dwell times (30 min per scan) can be used for these measurements because of the use of a lower-flux incident beam distributed over a significantly larger spot size. This allows for data collection to be performed to a much higher confidence level, with up to several orders of magnitude reduction in standard deviation.

The Mo K-edge PFY XAS spectrum (Figure S7) shows no significant changes at the edge under any of the employed conditions, in agreement with the collected Mo $K\alpha$ HERFD. The Fe K-edge PFY XAS measurements demonstrate a small degree of change similar to those observed using Fe $K\alpha$ HERFD, on the order of up to 1.5% in the case of E_1 (Figure 3). However, the drastic decrease in the standard error of these measurements makes such minor changes statistically significant (Figures 4 and S10−S13).

Changes are observed in three regions of the spectrum upon native reduction of MoFe from the E_0 to E_1 state. Namely, a decrease in the preedge intensity from ∼7109 to 7113 eV is
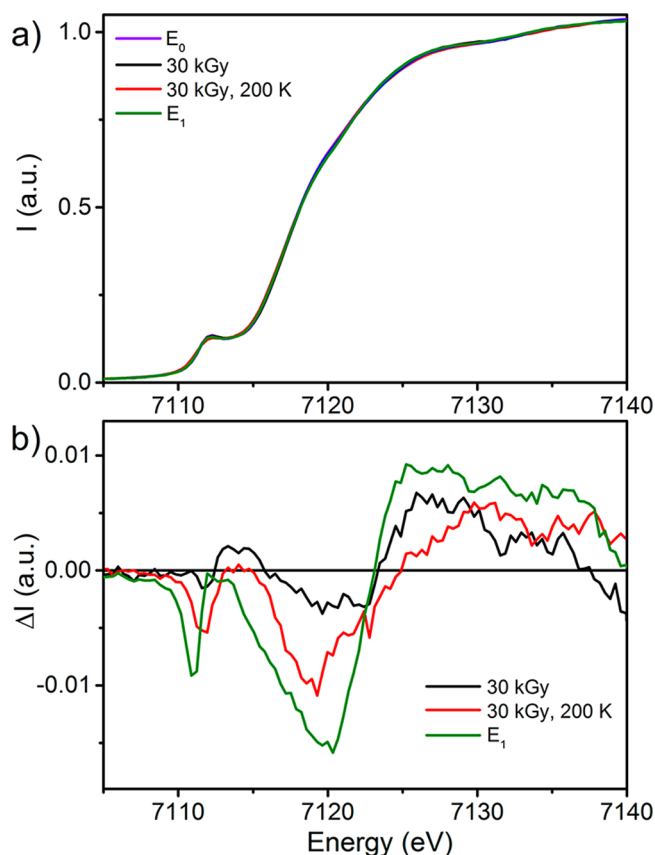
Figure 3. (Top) Comparison the Fe K-edge PFY XAS spectra of resting E_0 (violet), E_1 (green), 30 kGy, 200 K (red), and 30 kGy (black). (Bottom) Difference spectra generated by subtraction of the E_0 spectrum from the E_1 (green), 30 kGy (black), and 30 kGy, 200 K (red) spectra.
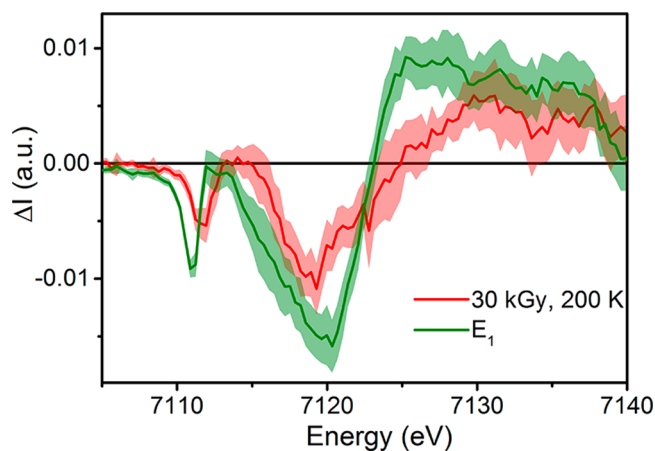

Figure 4. Comparison of the difference spectra generated by subtracting the Fe K-edge PFY spectrum of E_0 from either E_1 (green) or 30 kGy, 200 K (red). Standard deviations are shown as the partially transparent complimenting color. The 30 kGy spectrum is omitted here for clarity and is provided in section S4 of the Supporting Information.

accompanied by a decrease in the edge intensity from 7113 to 7123 eV and an increase at the white line above 7123 eV. The difference spectrum of $E_1 − E_0$ provides a reference for the changes expected in the spectra following both reduction and proton transfer, which can now be used to analyze the spectra resulting from the cryoreduction and annealing of MoFe.

As discussed above, the cryoreduction of MoFe also results in partial oxidation of the P cluster. Therefore, all presented cryoreduced XAS spectra are convoluted to some degree by the partial population of P^+. The Fe K-edge PFY XAS spectrum of P^{ox} was previously reported[60] and displayed a decrease in the white-line intensity, which was combined with a small increase in the intensity of both the preedge of ~7112 eV and the edge around 7120 eV (Figure S20). These changes are essentially counteractive to the differences observed in the E_1 spectrum, *particularly* at the white line. Therefore, it is not surprising that the 30 kGy cryoreduced sample exhibits only a small decrease in the edge intensity and a small increase in intensity at the white line, with no appreciable change at the preedge region. Upon annealing at 200 K, a decrease in the preedge intensity is observed along with a further decrease in the edge intensity to produce a spectrum similar to that of the native E_1 sample (as illustrated in Figure S15).

^{57}Fe Mössbauer Spectroscopy. To reconcile our current results from Fe XAS with those of the previous ^{57}Fe Mössbauer spectroscopy of cryoreduced and natively reduced MoFe,[46] we reinvestigated the ^{57}Fe Mössbauer spectroscopy of cryoreduced MoFe to see if the cryoreduction/annealing protocol would reproduce the original isomer shift observed for the E_1 state. While the XAS measurements observed *all* Fe present in the sample, ^{57}Fe Mössbauer spectroscopy *only* observed ^{57}Fe. Selective enrichment of the FeMoco cluster with ^{57}Fe can be accomplished by enriching MoFe with ^{57}Fe, extracting the enriched ^{57}FeMoco cluster, and reconstituting this cluster into unenriched ΔnifB FeMoco-deficient MoFe.[46,49] In this way, one can generate a Mössbauer sample that is solely sensitive to the FeMoco cluster. This was done previously,[46] and a sample of selectively enriched ^{57}FeMoco-enriched MoFe from this original study was obtained and measured in the resting, cryoreduced, and cryoreduced/200 K annealed states to gauge the change in the average isomer shift (δ_{avg}), and therefore Fe oxidation state, in these three states.

It is not surprising that very little change is observed between these three states, shown in Figure 5, because only a single-oxidation-state change at one of the seven Fe sites of FeMoco is expected. However, these small changes can still be quantified through fitting. A *unique* fit of the ^{57}Fe Mössbauer spectra of the FeMoco cluster requires a considerable amount of information that is currently unavailable for E_1, including an approximation of the individual Fe hyperfine tensors and their Euler angles. However, the average isomer shifts can still be obtained from the collapsed quadrupole spectra measured ~90 K using a minimalist fitting procedure to account for the absorption intensity (Figure S22). In this way, the spectra were adequately fit using two quadrupole doublets for the E_0 spectrum and three for the 30 kGy and 30 kGy, 200 K spectra. The results of these fits are summarized in Table 1.

The observed changes in the isomer shift are small but close to those expected based on previous findings.[46] Once the presence of E_0 in the 30 kGy and 30 kGy, 200 K samples is compensated for, we find a shift of +0.07 mm s^{-1} upon moving from E_0 to 30 kGy. This is slightly greater than that previously found for M^I, where +0.05 mm s^{-1} was observed with an unreported dose of radiation.[46] Upon annealing, the change in the isomer shift relative to E_0 is reduced to $\Delta\delta_{avg} = 0.02$ mm s^{-1}, similar to the previously reported species M^{Rg} (assigned as E_1).[46]
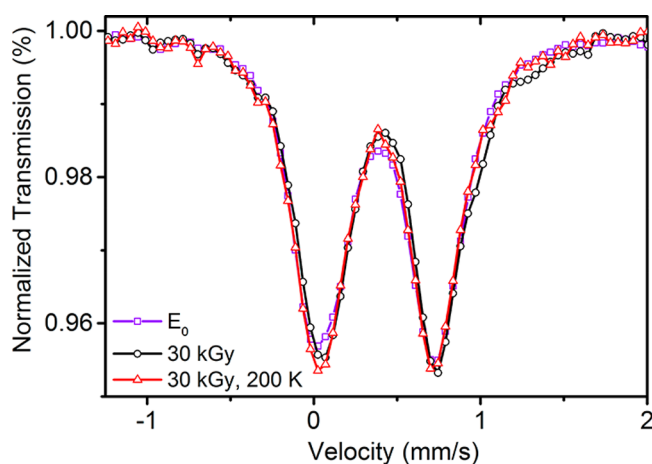
Figure 5. Comparison of the experimental resting E_0 (violet), 30 kGy (black), and 30 kGy, 200 K (red) ^{57}Fe Mössbauer spectra of a selectively ^{57}FeMoco/^{56}P-cluster-enriched MoFe sample. On the basis of EPR, the 30 kGy and 30 kGy, 200 K spectra contain ∼60% E_0. The spectra were collected under the following conditions: E_0 (100 K, 0 T), 30 kGy (90 K, 0.1 T), and 30 kGy, 200 K (90 K, 0 T). Errors and difference spectra are provided in section S6 of the Supporting Information.

Table 1. Summary of ^{57}Fe Mössbauer Fits of E_0, 30 kGy, and 30 kGy, 200 K Samples^a

	E_0	30 kGy	30 kGy, 200 K
$^b\delta$ (mm/s)	0.38	0.41	0.39
$^c\Delta\delta_{avg}$	0.00	0.03	0.01
$^d\Delta\delta_{avg}$	0.00	0.07	0.02

^{a}The average isomer shift of each species is formulated by the weighted average of the isomer shifts of its individual components. ^{b}Discrepancies in the absolute isomer shift of E_0 between the present and previous studies arise from the temperature-dependent second-order Doppler shift.[46] ^{c}Calculated by subtraction of $\delta(E_0)$. ^{d}Adjusted for the presence of E_0 (in the present samples, this was performed by multiplication of $\Delta\delta_{avg}$ by 2.5 to account for the ∼60% E_0 present).

4. DISCUSSION

Context of the E_1 Oxidation State. Few previous investigations have specifically aimed at exploring the electronic and geometric structures of the E_1 state of MoFe, and no conclusive evidence has been provided regarding the site of reduction on the FeMoco cluster in E_1.[66,67] To this end, perhaps the most significant effort undertaken to date involved the measurement of selectively ^{57}FeMoco-enriched MoFe using ^{57}Fe Mössbauer spectroscopy to ascertain the electronic properties of the catalytic cluster across a series of oxidation states.[46] More specifically, the one-electron-oxidized (M^{ox}), resting (M^N), low-flux turnover (5:1 [MoFe]/[FeP], referred to as "M^R"), and cryoreduced (M^I) states were measured and their isomer shifts δ determined. The isomer shift δ is diagnostic of Fe oxidation state, particularly for similar or identical complexes in a series of oxidation states. Considering that a typical change in the isomer shift ($\Delta\delta$) of ∼0.45 mm s^{-1} is observed upon moving from ferric to ferrous FeS$_4$, a change in the overall oxidation state of −1 for the seven Fe sites found in FeMoco is expected to produce an increase of 0.06 mm s^{-1} in the average isomer shift. This was indeed observed upon a comparison of the M^N and M^{ox} states. Similarly, M^I exhibited a similar change of $\Delta\delta \approx 0.05$ mm s^{-1} relative to M^N. However, a considerably smaller shift was seen upon a comparison of M^R

and M^N ($\Delta\delta \approx 0.02$ mm s^{-1}). The discrepancy of $\Delta\delta$ between M^I and M^R led to the proposal that M^I represented a unique species and that the series moving from M^{ox} to M^N to M^I involved sequential additions of electrons to the Fe centers of FeMoco. Meanwhile, the smaller $\Delta\delta$ observed in M^R was proposed, by inference, to be a Mo reduced state.[46] These results had significant implications, not only in that Mo, rather than Fe, was reduced in the E_1 state of MoFe but also in that the method of reduction determined the identity of the resulting species.

At the time of the study, it was generally accepted that the resting state of FeMoco contained Mo^{IV} based on previous ENDOR and XAS studies,[68−71] reasonably suggesting that native reduction could result in the formation of Mo^{III}. More recently, however, Mo $K\alpha$ HERFD and L-edge XAS have been used to demonstrate that the oxidation state of Mo in the resting E_0 state of Mo N2ase is best described as Mo^{III} in a non-Hund electronic configuration.[56,72] Therefore, if a Mo-centered reduction does indeed occur upon the initial reduction of the FeMoco cluster, a formal Mo^{II} center would be generated during native turnover.

Implications of Mo Redox Innocence. Because the Mo of FeMoco is the only Mo site in MoFe, the changes expected to occur upon reduction should be on the same order of magnitude as those observed upon comparison to reference Mo^{IV} and Mo^{III}, particularly in terms of the change in energy of the preedge and edge features (−1 eV for a one-electron reduction; section S3 of the Supporting Information). From the present Mo $K\alpha$ HERFD XAS spectrum (Figure 2), it is clear that no significant spectral changes occur at the Mo site of MoFe during native low-flux turnover or upon cryoreduction, which implies that Mo is not redox-active under the conditions utilized in this study.

Besides the implication of these results in assigning the oxidation state of Mo, we note that observing *no* significant changes in the preedge region of the spectrum was initially surprising based on the previous literature. More specifically, previous reports of the Mo and Fe K-edge extended X-ray absorption fine structure of MoFe under native turnover proposed that significant contractions of the Mo−Fe and Mo−O/N distances of −0.06 and −0.07 Å were found for the E_1 state.[67] It is already known that the Mo K-edge is fairly sensitive to the coordination environment,[64,73] and one would anticipate that such drastic changes in the first coordination sphere of Mo should result in noticeable changes in the preedge/edge features when measured using $K\alpha$ HERFD; however, none are observed here, implying that Mo coordination does not change upon formation of E_1. Unfortunately, the near-edge spectra (commonly referred to as XANES) were not reported in this previous study.

In a similar vein, it was hypothesized that homocitrate, which binds the Mo of FeMoco in the resting state, plays an essential role in proton relay to the FeMoco cluster during catalysis.[74] Computational studies on a model of the E_4 state of FeMoco have suggested that Mo may shift from 6- to 5-coordinate during turnover as the Mo-coordinating homocitrate becomes protonated.[75] Lowering of coordination would result in a lower approximate symmetry at Mo (from C_2 to C_1) and correspondingly an increase in the XAS preedge intensity. We do not observe any such changes presently, again suggesting that Mo remains 6-coordinate in E_1.

Fe K-Edge XAS of E_1 and Cryoreduced States. As indicated by the Fe K-edge PFY XAS spectra presented in

Figures 3 and 4, reduction of E_0 to E_1 results in a decrease in the intensity at both the preedge and edge regions and an increase in the intensity at the white line. Generally, the preedge feature of transitions metals with partially filled valence orbitals is expected to weaken as the oxidation state is decreased, assuming that no extreme perturbations in geometry or covalency occur.[76−78] It is well-established that fewer available holes in the metal d shell can result in a decrease in the intensity of the preedge feature. Thus, the results in Figures 3 and 4 are indicative that the E_1 state is generated through an Fe-centered reduction.

The position of the edge is another typical diagnostic of the metal oxidation state, which is expected to decrease in energy upon reduction (for an example, see Figure S16). Therefore, at face value the decreased intensity observed for E_1 in this region appears to indicate oxidation, which would contradict the interpretation of the changes that occur in the preedge region. However, there are several examples of FeS clusters that do not exhibit a change in energy at the edge region upon reduction.[60,61,79] This is often attributed to the high covalency of Fe−S bonds, where metal-centered oxidation state changes can be muted through changes in the Fe−S covalency[79−81] However, whether or not a shift in the edge position occurs upon reduction/oxidation of these systems also heavily depends on the mixed-valent nature of the new state being generated. As an example, the oxidation states at Fe in a symmetric $[2Fe−2S]^+$ cluster may appear as either $2Fe^{2.5+}$ or Fe^{III}/Fe^{II} depending on the degree of mixed valency (as well as experimental conditions in the case of Robin-Day class II[82] mixed-valent complexes). As a result, the edge of the XAS spectrum may appear either halfway between that of the $2Fe^{III}$ and $2Fe^{II}$ states (in the case of $2Fe^{2.5+}$) or as a convolution of the $2Fe^{III}$ and $2Fe^{II}$ states. In the latter case, the position of the edge will be dominated by the Fe^{II} center and will therefore appear at the same energy as the $2Fe^{II}$ dimer. This behavior has been previously characterized in the $[Et_4N]_n[LFe_2S_2]^{n−}$ ($n = 1$, 2, 3) series,[79] where the localized mixed-valent character of the $n = 2$ species results in the same edge energy as the $n = 3$ species in this complex (Figure S19). This is nearly identical with what we observe in Figures 3 and 4 for the E_1 state, rationalizing the observed decrease in the edge intensity and further supporting an Fe-based reduction in E_1.

Last, the white-line region generally results from strongly allowed electronic transitions that are confined to the vicinity of the absorbing atom or low-energy continuum states confined by strong multiple scattering. These states are difficult to predict and thus are less well understood than the transitions that contribute to the preedge and edge regions. However, this region can still be used as a fingerprint for the chemical bonding, oxidation state, and three-dimensional environment of the absorber. This region has been seen to increase in intensity with decreasing oxidation state not only for FeP and the P cluster[60,80] but also in FeS model complexes.[61,79] The changes that occur in the white line of the Fe XANES spectrum upon formation of E_1 are therefore also consistent with an Fe-centered reduction.

With our consideration of E_1 formed during native turnover in hand, we now turn to the cryoreduced species. Similar to E_1, a decrease in the edge intensity coupled with an increase in the white-line intensity is seen in the 30 kGy sample, albeit to a smaller degree. It is notable that there is no significant decrease in the preedge intensity. Meanwhile, annealing of the 30 kGy cryoreduced sample results in a decreased preedge intensity, as

well as a further decrease in the edge intensity. This produces a difference spectrum that is very similar to that of the E_1 state (Figure 3). While some discrepancies do exist, particularly in the degree to which the intensities of the preedge and edge are decreased, it is important to keep in mind that ∼7% of the P cluster in these cryoreduced samples is present as P^+. On the basis of previous XAS studies of P^N/P^+, any P^+ present is expected to increase the preedge and edge intensities, while significantly decreasing the white-line intensity (Figure S20).[60] These contributions directly correlate with the discrepancies between the E_1 and 30 kGy, 200 K samples. This further supports the hypothesis that the differences between the cryoreduced and E_1 states are not due to Fe versus Mo reduction but instead to the fact that the cryoreduced state has not yet acquired a proton (Scheme 1).

These results are further corroborated by the ^{57}Fe Mössbauer spectroscopy results. Similar to the previously reported study of cryoreduced MoFe, we observe a change in the isomer shift of $\Delta\delta_{avg} = 0.07$ mm $s^{−1}$ following cryoreduction using 30 kGy of radiation once the remaining contributions of E_0 are accounted for (compared to the 0.05 mm $s^{−1}$ produced using an unspecified dose). Because there are seven Fe sites present in FeMoco, this corresponds to a $\Delta\delta_{avg} = 0.49$ mm $s^{−1}$ at a single Fe site, consistent with an Fe-centered reduction. This is not intended to imply that this additional electron is fully delocalized over all seven Fe sites. Annealing of this sample at 200 K produces a shift of $\Delta\delta_{avg} = 0.02$ mm $s^{−1}$, identical with that observed previously for E_1.[46] This is equivalent to a much smaller $\Delta\delta_{avg} = 0.14$ mm $s^{−1}$ shift for a single Fe site. This considerably smaller shift is intriguing because it implies that the additional electron contained in the E_1 state is either fairly delocalized, involved in a highly covalent interaction, or both. Whether this can be attributed to iron hydride formation or the protonation of one of the S atoms in FeMoco remains unclear. What is perhaps clearer is that in either scenario the reducing equivalent appears to be distributed in such a manner as to minimize the apparent change in the oxidation state of the cluster, supporting the hypothesis that protonation of the cluster serves to level its reduction potential.

Thus far, the Fe K-edge XAS and ^{57}Fe Mössbauer spectroscopy results support that (a) E_1 trapped during turnover consists of an Fe-reduced state and (b) annealing of the cryoreduced state produces E_1. Why then does the E_1 state appear more reduced in the Fe K-edge XAS, while the cryoreduced state appears more reduced in the ^{57}Fe Mössbauer spectroscopy? This is partially explained by the presence of ∼7% P^+ in the cryoreduced samples that is observed in the XAS but not in the Mössbauer spectroscopy. However, even though the 30 kGy and 30 kGy, 200 K samples both contain the same contribution from P^+, the 30 kGy, 200 K sample still appears more reduced in the XAS and less reduced in the Mössbauer spectroscopy. This implies that more must occur at the FeMoco cluster to generate E_1 than simply the transfer of an electron and a proton; rather, it appears that a degree of electronic reorganization is also necessary. This kind of phenomenon has already been observed in previous cryoreduction studies of MoFe, where cryoreduction of the samples of E_1 resulted in a unique $S = {}^1/_2$ species rather than the $S = {}^3/_2$ species of E_2[45] and may very well occur here.

5. CONCLUSIONS

The present study has interrogated the behavior of both Mo and Fe of MoFe under both low-flux turnover and cryoreducing conditions. The results of the Mo Kα HERFD XAS demonstrate clearly that one-electron reduction of MoFe does not result in a Mo-centered reduction under either of these conditions. Fe K-edge XAS measurements further demonstrate that an Fe-centered redox event occurs under both native turnover and cryoreducing conditions, which is attributable to the FeMoco cluster on the basis of EPR. The changes observed upon moving from E_0 to E_1 are consistent with the one-electron reduction of Fe at FeMoco. While only minor changes are observed in the Fe K-edge XAS of MoFe following 30 kGy of irradiation, annealing of this sample for 2 min at 200 K generates a species closely related to E_1. The differences between E_1 and this cryoreduced/annealed species is accounted for by the presence of P^+ in the latter, which is also generated during cryoreduction. These results are further supported by ^{57}Fe Mössbauer spectroscopy, where the same change in the isomer shift $\Delta\delta_{avg}$ as that previously reported for the E_1 state is observed following cryoreduction/annealing. On these bases, our results support the hypothesis that the states of FeMoco in cryoreduced MoFe and natively reduced E_1 are related to one another through proton transfer. Building from previous studies, we propose that the metal valencies of the E_1 state follow a $[Mo^{III}4Fe^{II}3Fe^{III}]$ distribution.

The present work provides significant insight into the nature of the E_1 state of MoFe and clearly establishes the redox innocence of Mo in the reduction of resting state (E_0) N2ase to the E_1 state. This work demonstrates that Fe is reduced in the E_1 state and that both low-flux turnover and cryoreduction can function as a route to populating this state. These results provide crucial information for mechanistic studies in terms of possible electron distributions and variation in the coordination environment of the metal centers of the catalytic cluster and serve as a guide for further studies regarding the precise nature of E_1.

ASSOCIATED CONTENT

ⓢ Supporting Information

The Supporting Information is available free of charge on the ACS Publications website at DOI: 10.1021/acs.inorg-chem.9b01951.

Preparation of the reference model complexes and more detailed spectroscopic data and analysis (PDF)

AUTHOR INFORMATION

Corresponding Author

*E-mail: serena.debeer@cec.mpg.de.

ORCID ⓞ

Casey Van Stappen: 0000-0002-1770-2231
Zhi-Yong Yang: 0000-0001-8186-9450
Yisong Guo: 0000-0002-4132-3565
Eckhard Bill: 0000-0001-9138-3964
Lance C. Seefeldt: 0000-0002-6457-9504
Brian M. Hoffman: 0000-0002-3100-0746
Serena DeBeer: 0000-0002-5196-3400

Notes

The authors declare no competing financial interest.

REFERENCES

(1) Smil, V. *Enriching the Earth: Fritz Haber, Carl Bosch, and the Transformation of World Food Production*; MIT Press: Cambridge, MA, 2001.

(2) Boyd, E. S.; Anbar, A. D.; Miller, S.; Hamilton, T. L.; Lavin, M.; Peters, J. W. A late methanogen origin for molybdenum-dependent nitrogenase. *Geobiology* **2011**, *9*, 221−32.

(3) Burgess, B. K.; Lowe, D. J. Mechanism of Molybdenum Nitrogenase. *Chem. Rev.* **1996**, *96*, 2983−3012.

(4) Hoffman, B. M.; Lukoyanov, D.; Yang, Z.-Y.; Dean, D. R.; Seefeldt, L. C. Mechanism of Nitrogen Fixation by Nitrogenase: The Next tage. *Chem. Rev.* **2014**, *114*, 4041−62.

(5) Bulen, W. A.; LeComte, J. R. The nitrogenase system from Azotobacter: two-enzyme requirement for N2 reduction, ATP-dependent H2 evolution, and ATP hydrolysis. *Proc. Natl. Acad. Sci. U.S.A.* **1966**, *56*, 979−986.

(6) Chatt, J.; Dilworth, J. R.; Richards, R. L. Recent Advances in the Chemistry of Nitrogen Fixation. *Chem. Rev.* **1978**, *78*, 589−625.

(7) Hussain, W.; Leigh, G. J.; Pickett, C. J. Stepwise Conversion of Dinitrogen Co-ordinated to Molybdenum into an Amine and an Imido-complex. Relevance to the Reactions of Nitrogenase. *J. Chem. Soc., Chem. Commun.* **1982**, 747−748.

(8) Pickett, C. J. The Chatt cycle and the mechanism of enzymic reduction of molecular nitrogen. *JBIC, J. Biol. Inorg. Chem.* **1996**, *1*, 601−606.

(9) Schrock, R. R. Catalytic Reduction of Dinitrogen to Ammonia at a Single Molybdenum Center. *Acc. Chem. Res.* **2005**, *38*, 955−62.

(10) Yandulov, D. V.; Schrock, R. R. Reduction of Dinitrogen to Ammonia at a Well-Protected Reaction Site in a Molybdenum Triamidoamine Complex. *J. Am. Chem. Soc.* **2002**, *124*, 6252−6253.

(11) Shilov, A. E. Catalytic reduction of dinitrogen in protic media: chemical models of nitrogenase. *J. Mol. Catal.* **1987**, *41*, 221−234.

(12) Yandulov, D. V.; Schrock, R. R. Catalytic Reduction of Dinitrogen to Ammonia at a Single Molybdenum Center. *Science* **2003**, *301*, 76−8.

(13) Lee, S. C.; Holm, R. H. The Clusters of Nitrogenase: Synthetic Methodology in the Construction of Weak-Field Clusters. *Chem. Rev.* **2004**, *104*, 1135−58.

(14) Malinak, S. M.; Coucouvanis, D. The Chemistry of Synthetic Fe-Mo-S Clusters and their Relevance to the Structure and Function of the Fe-Mo-S Center in Nitrogenase. *Prog. Inorg. Chem.* **2007**, *49*, 599−662.

(15) Arashiba, K.; Miyake, Y.; Nishibayashi, Y. A molybdenum complex bearing PNP-type pincer ligands leads to the catalytic reduction of dinitrogen into ammonia. *Nat. Chem.* **2011**, *3*, 120−5.

(16) Arashiba, K.; Nakajima, K.; Nishibayashi, Y. Synthesis and Reactivity of Molybdenum-Dinitrogen Complexes Bearing PNN-Type Pincer Ligand. *Z. Anorg. Allg. Chem.* **2015**, *641*, 100−104.

(17) Itabashi, T.; Mori, I.; Arashiba, K.; Eizawa, A.; Nakajima, K.; Nishibayashi, Y. Effect of substituents on molybdenum triiodide complexes bearing PNP-type pincer ligands toward catalytic nitrogen fixation. *Dalton Trans.* **2019**, *48*, 3182−3186.

(18) Jia, H. P.; Quadrelli, E. A. Mechanistic aspects of dinitrogen cleavage and hydrogenation to produce ammonia in catalysis and organometallic chemistry: relevance of metal hydride bonds and dihydrogen. *Chem. Soc. Rev.* **2014**, *43*, 547−64.

(19) Khoenkhoen, N.; de Bruin, B.; Reek, J. N. H.; Dzik, W. I. Reactivity of Dinitrogen Bound to Mid- and Late-Transition-Metal Centers. *Eur. J. Inorg. Chem.* **2015**, *2015*, 567−598.

(20) Kuriyama, S.; Arashiba, K.; Nakajima, K.; Tanaka, H.; Kamaru, N.; Yoshizawa, K.; Nishibayashi, Y. Catalytic formation of Ammonia from Molecular Dinitrogen by Use of Dinitrogen-Bridged Dimolybdenum-Dinitrogen Complexes Bearing PNP-pincer Ligands: Remarkable Effect of Substituent at PNP-Pincer Ligand. *J. Am. Chem. Soc.* **2014**, *136*, 9719−31.

(21) Kuriyama, S.; Arashiba, K.; Nakajima, K.; Tanaka, H.; Yoshizawa, K.; Nishibayashi, Y. Nitrogen fixation catalyzed by ferrocene-substituted dinitrogen-bridged dimolybdenum-dinitrogen complexes: unique behavior of ferrocene moiety as redox active site. *Chem. Sci.* **2015**, *6*, 3940−3951.

(22) Nishibayashi, Y. *Transition Metal−Dinitrogen Complexes: Preparation and Reactivity*; Wiley-VCH, 2019; p 496.

(23) Spatzal, T.; Perez, K. A.; Einsle, O.; Howard, J. B.; Rees, D. C. Ligand binding to the FeMo-cofactor: structures of CO-bound and reactivated nitrogenase. *Science* **2014**, *345*, 1620−3.

(24) Pollock, R. C.; Lee, H.-I.; Cameron, L. M.; DeRose, V. J.; Hales, B. J.; Orme-Johnson, W. H.; Hoffman, B. M. Investigation of CO Bound to Inhibited Forms of Nitrogenase MoFe Protein by ^{13}C ENDOR. *J. Am. Chem. Soc.* **1995**, *117*, 8686−8687.

(25) Barney, B. M.; Igarashi, R. Y.; Dos Santos, P. C.; Dean, D. R.; Seefeldt, L. C. Substrate Interaction at an Iron-Sulfur Face of the FeMo-cofactor during Nitrogenase Catalysis. *J. Biol. Chem.* **2004**, *279*, 53621−53624.

(26) Barney, B. M.; Laryukhin, M.; Igarashi, R. Y.; Lee, H.-I.; Dos Santos, P. C.; Yang, T.-C.; Hoffman, B. M.; Dean, D. R.; Seefeldt, L. C. Trapping a Hydrazine Reduction Intermediate on the Nitrogenase Active Site. *Biochemistry* **2005**, *44*, 8030−7.

(27) Barney, B. M.; Lukoyanov, D.; Igarashi, R. Y.; Laryukhin, M.; Yang, T.-C.; Dean, D. R.; Hoffman, B. M.; Seefeldt, L. C. Trapping an intermediate of dinitrogen (N_2) reduction on nitrogenase. *Biochemistry* **2009**, *48*, 9094−102.

(28) Barney, B. M.; Lukoyanov, D.; Yang, T.-C.; Dean, D. R.; Hoffman, B. M.; Seefeldt, L. C. A methyldiazene (HN=N-CH$_3$)-derived species bound to the nitrogenase active-site FeMo cofactor: Implications for mechanism. *Proc. Natl. Acad. Sci. U. S. A.* **2006**, *103*, 17113−8.

(29) Lowe, D. J.; Thorneley, R. N. F. The mechanism of Klebsiella pneumoniae nitrogenase action. Pre-steady-state kinetics of H$_2$ formation. *Biochem. J.* **1984**, *224*, 877−86.

(30) Lowe, D. J.; Thorneley, R. N. F. The mechanism of Klebsiella pneumoniae nitrogenase action. The determination of rate constants required for the simulation of the kinetics of N_2 reduction and H$_2$ evolution. *Biochem. J.* **1984**, *224*, 895−901.

(31) Thorneley, R. N. F.; Lowe, D. J. The mechanism of Klebsiella pneumoniae nitrogenase action. Pre-steady-state kinetics of an enzyme-bound intermediate in N_2 reduction and of NH$_3$ formation. *Biochem. J.* **1984**, *224*, 887−94.

(32) Thorneley, R. N. F.; Lowe, D. J. The mechanism of Klebsiella pneumoniae nitrogenase action. Simulation of the dependences of H$_2$-evolution rate on component-protein concentration and ratio and sodium dithionite concentration. *Biochem. J.* **1984**, *224*, 903−9.

(33) Burgess, B. K.; Wherland, S.; Newton, W. E.; Stiefel, E. I. Nitrogenase Reactivity: Insight into the Nitrogen-Fixing Process through Hydrogen-Inhibition and HD-Forming Reactions. *Biochemistry* **1981**, *20*, 5140−5146.

(34) Guth, J. H.; Burris, R. H. Inhibition of Nitrogenase-Catalyzed NH$_3$ Formation by H$_2$. *Biochemistry* **1983**, *22*, 5111−5122.

(35) Rivera-Ortiz, J. M.; Burris, R. H. Interactions Among Substrates and Inhibitors of Nitrogenase. *J. Bacteriol.* **1975**, *123*, 537−545.

(36) Watt, G. D.; Bulen, W. A.; Burns, A.; Hadfield, K. L. Stoichiometry, ATP/2e Values, and Energy Requirements for Reactions Catalyzed by Nitrogenase from Azotobacter vinelandii. *Biochemistry* **1975**, *14*, 4266−4272.

(37) Lukoyanov, D.; Khadka, N.; Yang, Z.-Y.; Dean, D. R.; Seefeldt, L. C.; Hoffman, B. M. Reductive Elimination of H$_2$ Activates Nitrogenase to Reduce the N≡N Triple Bond: Characterization of the E$_4$(4H) Janus Intermediate in Wild-Type Enzyme. *J. Am. Chem. Soc.* **2016**, *138*, 10674−83.

(38) Lukoyanov, D. A.; Khadka, N.; Yang, Z.-Y.; Dean, D. R.; Seefeldt, L. C.; Hoffman, B. M. Hydride Conformers of the Nitrogenase FeMo-cofactor Two-Electron Reduced State E$_2$(2H), Assigned Using Cryogenic Intra Electron Paramagnetic Resonance Cavity Photolysis. *Inorg. Chem.* **2018**, *57*, 6847−6852.

(39) Brown, K. A.; Harris, D. F.; Wilker, M. B.; Rasmussen, A.; Khadka, N.; Hamby, H.; Keable, S.; Dukovic, G.; Peters, J. W.; Seefeldt, L. C.; King, P. W. Light-driven dinitrogen reduction catalyzed by a CdS:nitrogenase MoFe protein biohybrid. *Science* **2016**, *352*, 448−50.

(40) Danyal, K.; Rasmussen, A. J.; Keable, S. M.; Inglet, B. S.; Shaw, S.; Zadvornyy, O. A.; Duval, S.; Dean, D. R.; Raugei, S.; Peters, J. W.; Seefeldt, L. C. Fe Protein-Independent Substrate Reduction by Nitrogenase MoFe Protein Variants. *Biochemistry* **2015**, *54*, 2456−62.

(41) Paengnakorn, P.; Ash, P. A.; Shaw, S.; Danyal, K.; Chen, T.; Dean, D. R.; Seefeldt, L. C.; Vincent, K. A. Infrared spectroscopy of the nitrogenase MoFe protein under electrochemical control: potential-triggered CO binding. *Chem. Sci.* **2017**, *8*, 1500−1505.

(42) Roth, L. E.; Tezcan, F. A. ATP-Uncoupled, Six-Electron Photoreduction of Hydrogen Cyanide to Methane by the Molybdenum−Iron Protein. *J. Am. Chem. Soc.* **2012**, *134*, 8416−8419.

(43) Roth, L. E.; Nguyen, J. C.; Tezcan, F. A. ATP- and Iron-Protein-Independent Activation of Nitrogenase Catalysis by Light. *J. Am. Chem. Soc.* **2010**, *132*, 13672−13674.

(44) Davydov, R.; Hoffman, B. M. Active intermediates in heme monooxygenase reactions as revealed by cryoreduction/annealing, EPR/ENDOR studies. *Arch. Biochem. Biophys.* **2011**, *507*, 36−43.

(45) Davydov, R.; Khadka, N.; Yang, Z.-Y.; Fielding, A. J.; Lukoyanov, D.; Dean, D. R.; Seefeldt, L. C.; Hoffman, B. M. Exploring Electron/Proton Transfer and Conformational Changes in the Nitrogenase MoFe Protein and FeMo-cofactor Through Cryoreduction/EPR Measurements. *Isr. J. Chem.* **2016**, *56*, 841−851.

(46) Yoo, S. J.; Angove, H. C.; Papaefthymiou, V.; Burgess, B. K.; Münck, E. Mössbauer Study of the MoFe Protein of Nitrogenase from Azotobacter vinelandii Using Selective ^{57}Fe Enrichment of the M-Centers. *J. Am. Chem. Soc.* **2000**, *122*, 4926−4936.

(47) Igarashi, R. Y.; Laryukhin, M.; Dos Santos, P. C.; Lee, H.-I.; Dean, D. R.; Seefeldt, L. C.; Hoffman, B. M. Trapping H$^-$ Bound to the Nitrogenase FeMo-Cofactor Active Site during H$_2$ Evolution: Characterization by ENDOR Spectroscopy. *J. Am. Chem. Soc.* **2005**, *127*, 6231−41.

(48) Doan, P. E.; Telser, J.; Barney, B. M.; Igarashi, R. Y.; Dean, D. R.; Seefeldt, L. C.; Hoffman, B. M. ^{57}Fe ENDOR spectroscopy and 'Electron Inventory' Analysis of the Nitrogenase E$_4$ Intermediate

Suggest the Metal-Ion Core of FeMo-Cofactor Cycles Through Only One Redox Couple. *J. Am. Chem. Soc.* **2011**, *133*, 17329−40.

(49) Christiansen, J.; Goodwin, P. J.; Lanzilotta, W. N.; Seefeldt, L. C.; Dean, D. R. Catalytic and Biophysical Properties of a Nitrogenase Apo-MoFe Protein Produced by a nifB-Deletion Mutant of Azotobacter vinelandii†. *Biochemistry* **1998**, *37*, 12611−12623.

(50) Solé, V. A.; Papillon, E.; Cotte, M.; Walter, P.; Susini, J. A multiplatform code for the analysis of energy-dispersive X-ray fluorescence spectra. *Spectrochim. Acta, Part B* **2007**, *62*, 63−68.

(51) Ravel, B.; Newville, M. ATHENA, ARTEMIS, HEPHAESTUS: data analysis for X-ray absorption spectroscopy using IFEFFIT. *J. Synchrotron Radiat.* **2005**, *12*, 537−41.

(52) Cutsail, G. E., 3rd; Banerjee, R.; Zhou, A.; Que, L., Jr.; Lipscomb, J. D.; DeBeer, S. High-Resolution Extended X-ray Absorption Fine Structure Analysis Provides Evidence for a Longer Fe-Fe Distance in the Q Intermediate of Methane Monooxygenase. *J. Am. Chem. Soc.* **2018**, *140*, 16807−16820.

(53) Castillo, R. G.; Banerjee, R.; Allpress, C. J.; Rohde, G. T.; Bill, E.; Que, L., Jr.; Lipscomb, J. D.; DeBeer, S. High-Energy-Resolution Fluorescence-Detected X-ray Absorption of the Q Intermediate of Soluble Methane Monooxygenase. *J. Am. Chem. Soc.* **2017**, *139*, 18024−18033.

(54) Lukoyanov, D.; Yang, Z.-Y.; Duval, S.; Danyal, K.; Dean, D. R.; Seefeldt, L. C.; Hoffman, B. M. A Confirmation of the Quench-Cryoannealing Relaxation Protocol for Identifying Reduction States of Freeze-Trapped Nitrogenase Intermediates. *Inorg. Chem.* **2014**, *53*, 3688−93.

(55) Tittsworth, R. C.; Hales, B. J. Detection of EPR Signals Assigned to the 1-equiv-Oxidized P-Clusters of the Nitrogenase MoFe-Protein from Azotobacter vinelandii. *J. Am. Chem. Soc.* **1993**, *115*, 9763−9767.

(56) Bjornsson, R.; Lima, F. A.; Spatzal, T.; Weyhermüller, T.; Glatzel, P.; Bill, E.; Einsle, O.; Neese, F.; DeBeer, S. Identification of a spin-coupled Mo(III) in the nitrogenase iron-molybdenum cofactor. *Chem. Sci.* **2014**, *5*, 3096−3103.

(57) Danyal, K.; Dean, D. R.; Hoffman, B. M.; Seefeldt, L. C. Electron Transfer within Nitrogenase: Evidence for a Deficit-Spending Mechanism. *Biochemistry* **2011**, *50*, 9255−63.

(58) Danyal, K.; Mayweather, D.; Dean, D. R.; Seefeldt, L. C.; Hoffman, B. M. Conformational Gating of Electron Transfer from the Nitrogenase Fe Protein to MoFe Protein. *J. Am. Chem. Soc.* **2010**, *132*, 6894−5.

(59) Yang, Z.-Y.; Ledbetter, R.; Shaw, S.; Pence, N.; Tokmina-Lukaszewska, M.; Eilers, B.; Guo, Q.; Pokhrel, N.; Cash, V. L.; Dean, D. R.; Antony, E.; Bothner, B.; Peters, J. W.; Seefeldt, L. C. Evidence That the P_i Release Event Is the Rate-Limiting Step in the Nitrogenase Catalytic Cycle. *Biochemistry* **2016**, *55*, 3625−35.

(60) Musgrave, K. B.; Liu, H. I.; Ma, L.; Burgess, B. K.; Watt, G.; Hedman, B.; Hodgson, K. O. EXAFS studies on the P^N and P^{OX} states of the P-clusters in nitrogenase. *JBIC, J. Biol. Inorg. Chem.* **1998**, *3*, 344−352.

(61) Rees, J. A.; Bjornsson, R.; Kowalska, J. K.; Lima, F. A.; Schlesier, J.; Sippel, D.; Weyhermuller, T.; Einsle, O.; Kovacs, J. A.; DeBeer, S. Comparative electronic structures of nitrogenase FeMoco and FeVco. *Dalton Trans.* **2017**, *46*, 2445−2455.

(62) Eisenberger, P.; Platzman, P. M.; Winick, H. X-Ray Resonant Raman Scattering: Observation of Characteristic Radiation Narrower than the Lifetime Width. *Phys. Rev. Lett.* **1976**, *36*, 623−626.

(63) Glatzel, P.; Sikora, M.; Smolentsev, G.; Fernández-García, M. Hard X-ray photon-in photon-out spectroscopy. *Catal. Today* **2009**, *145*, 294−299.

(64) Lima, F. A.; Bjornsson, R.; Weyhermuller, T.; Chandrasekaran, P.; Glatzel, P.; Neese, F.; DeBeer, S. High-resolution molybdenum K-edge X-ray absorption spectroscopy analyzed with time-dependent density functional theory. *Phys. Chem. Chem. Phys.* **2013**, *15*, 20911−20.

(65) Glatzel, P.; Bergmann, U. High resolution 1s core hole X-ray spectroscopy in 3d transition metal complexes—electronic and structural information. *Coord. Chem. Rev.* **2005**, *249*, 65−95.

(66) Yoo, S. J.; Angove, H. C.; Burgess, B. K.; Hendrich, M. P.; Münck, E. Mössbauer and Integer-Spin EPR Studies and Spin-Coupling Analysis of the $[4Fe-4S]^0$ Cluster of the Fe Protein from Azotobacter vinelandii Nitrogenase. *J. Am. Chem. Soc.* **1999**, *121*, 2534−2545.

(67) Christiansen, J.; Tittsworth, R. C.; Hales, B. J.; Cramer, S. P. Fe and Mo EXAFS of Azotobacter vinelandii Nitrogenase in Partially Oxidized and Singly Reduced Forms. *J. Am. Chem. Soc.* **1995**, *117*, 10017−10024.

(68) Hedman, B.; Frank, P.; Gheller, S. F.; Roe, A. L.; Newton, W. E.; Hodgson, K. O. New Structure Insights into the Iron-Molybdenum Cofactor from Azotobacter vinelandii Nitrogenase through Sulfur K and Molybdenum L X-ray Absorption Edge Studies. *J. Am. Chem. Soc.* **1988**, *110*, 3798−3805.

(69) Hoffman, B. M.; Roberts, J. E.; Orme-Johnson, W. H. ^{95}Mo and ^{1}H ENDOR Spectroscopy of the Nitrogenase MoFe Protein. *J. Am. Chem. Soc.* **1982**, *104*, 860−862.

(70) True, A. E.; McLean, P.; Nelson, M. J.; Orme-Johnson, W. H.; Hoffman, B. M. Comparison of Wild-Type and nifV Mutant Molybdenum-Iron Proteins of Nitrogenase from Klebsiella pneumoniae by ENDOR Spectroscopy. *J. Am. Chem. Soc.* **1990**, *112*, 651−657.

(71) Venters, R. A.; Nelson, M. J.; McLean, P. A.; True, A. E.; Levy, M. A.; Hoffman, B. M.; Orme-Johnson, W. H. ENDOR of the Resting State of Nitrogenase Molybdenum-Iron Proteins from Azotobacter vinelandii, Klebsiella pneumoniae, and Clostridium pasteurianum: ^{1}H, ^{57}Fe, ^{95}Mo, and ^{33}S Studies. *J. Am. Chem. Soc.* **1986**, *108*, 3487−3498.

(72) Bjornsson, R.; Delgado-Jaime, M. U.; Lima, F. A.; Sippel, D.; Schlesier, J.; Weyhermüller, T.; Einsle, O.; Neese, F.; DeBeer, S. Molybdenum L-Edge XAS Spectra of MoFe Nitrogenase. *Z. Anorg. Allg. Chem.* **2015**, *641*, 65−71.

(73) Conradson, S. D.; Burgess, B. K.; Newton, W. E.; Hodgson, K. O.; McDonald, J. W.; Rubinson, J. F.; Gheller, S. F.; Mortenson, L. E.; Adams, M. W. W.; Mascharak, P. K.; Armstrong, W. A.; Holm, R. H. Structural Insights from the Mo K-edge X-ray Absorption Near Edge Structure of the Iron-Molybdenum Protein of Nitrogenase and Its Iron-Molybdenum Cofactor by Comparison with Synthetic Fe-Mo-S Clusters. *J. Am. Chem. Soc.* **1985**, *107*, 7935−7940.

(74) Dance, I. The pathway for serial proton supply to the active site of nitrogenase: enhanced density functional modeling of the Grotthuss mechanism. *Dalton Trans.* **2015**, *44*, 18167−86.

(75) Siegbahn, P. E. M. A Major Structural Change of the Homocitrate Ligand of Probable Importance for the Nitrogenase Mechanism. *Inorg. Chem.* **2018**, *57*, 1090−1095.

(76) Chandrasekaran, P.; Stieber, S. C.; Collins, T. J.; Que, L., Jr.; Neese, F.; DeBeer, S. Prediction of high-valent iron K-edge absorption spectra by time-dependent Density Functional Theory. *Dalton Trans.* **2011**, *40*, 11070−9.

(77) DeBeer George, S.; Brant, P.; Solomon, E. I. Metal and Ligand K-edge XAS of Organotitanium complexes: Metal 4p and 3d Contributions to Pre-edge Intensity and Their Contributions to Bonding. *J. Am. Chem. Soc.* **2005**, *127*, 667−74.

(78) Westre, T. E.; Kennepohl, P.; DeWitt, J. G.; Hedman, B.; Hodgson, K. O.; Solomon, E. I. A Multiplet Analysis of Fe K-Edge 1s → 3d Pre-edge Features of Iron Complexes. *J. Am. Chem. Soc.* **1997**, *119*, 6297−6314.

(79) Kowalska, J. K.; Hahn, A. W.; Albers, A.; Schiewer, C. E.; Bjornsson, R.; Lima, F. A.; Meyer, F.; DeBeer, S. X-ray Absorption and Emission Spectroscopic Studies of $[L_2Fe_2S_2]^n$ Model Complexes: Implications for the Experimental Evaluation of Redox States in Iron-Sulfur Clusters. *Inorg. Chem.* **2016**, *55*, 4485−97.

(80) Musgrave, K. B.; Angove, H. C.; Burgess, B. K.; Hedman, B.; Hodgson, K. O. All-Ferrous Titanium(III) Citrate Reduced Fe Protein of Nitrogenase: An XAS Study of Electronic and Metrical Structure. *J. Am. Chem. Soc.* **1998**, *120*, 5325−5326.

(81) Lugo-Mas, P.; Dey, A.; Xu, L.; Davin, S. D.; Benedict, J.; Kaminsky, W.; Hodgson, K. O.; Hedman, B.; Solomon, E. I.; Kovacs, J. A. How Does Single Oxygen Atom Addition Affect the Properties of

an Fe-Nitrile Hydratase Analogue? The Compensatory Role of the Unmodified Thiolate. *J. Am. Chem. Soc.* **2006**, *128*, 11211−21.

(82) Robin, M. B.; Day, P. Mixed Valence Chemistry - A Survey and Classification. *Adv. Inorg. Chem. Radiochem.* **1968**, *10*, 247−422.